Bone mineral and stiffness loss at the distal femur and proximal tibia in acute spinal cord injury

W. B. Edwards · T. J. Schnitzer · K. L. Troy

Abstract

Summary Computed tomography and finite element modeling were used to assess bone mineral and stiffness loss at the knee following acute spinal cord injury (SCI). Marked bone mineral loss was observed from a combination of trabecular and endocortical resorption. Reductions in stiffness were 2-fold greater than reductions in integral bone mineral.

Introduction SCI is associated with a rapid loss of bone mineral and an increased rate of fragility fracture. The large majority of these fractures occur around regions of the knee. Our purpose was to quantify changes to bone mineral, geometry, strength indices, and stiffness at the distal femur and proximal tibia in acute SCI.

Methods Quantitative computed tomography (QCT) and patient-specific finite element analysis were performed on 13 subjects with acute SCI at serial time points separated by a mean of 3.5 months (range 2.6–4.8 months). Changes in bone mineral content (BMC) and volumetric bone mineral density (vBMD) were quantified for integral, trabecular, and cortical bone at epiphyseal, metaphyseal, and diaphyseal regions of the distal femur and proximal tibia. Changes in bone volumes, cross-sectional areas, strength indices and stiffness were also determined.

Results Bone mineral loss was similar in magnitude at the distal femur and proximal tibia. Reductions were most pronounced at epiphyseal regions, ranging from 3.0 % to 3.6 % per month for integral BMC ($p < 0.001$) and from 2.8 % to 3.4 % per month ($p < 0.001$) for integral vBMC. Trabecular BMC decreased by 3.1–4.4 %/month ($p < 0.001$) and trabecular vBMD by 2.7–4.7 %/month ($p < 0.001$). A 3.8–5.4 %/month reduction was observed for cortical BMC ($p < 0.001$); the reduction in cortical vBMD was noticeably lower (0.6–0.8 %/month; $p \leq 0.01$). The cortical bone loss occurred primarily through endosteal resorption, and reductions in strength indices and stiffness were some 2-fold greater than reductions in integral bone mineral.

Conclusions These findings highlight the need for therapeutic interventions targeting both trabecular and endocortical bone mineral preservation in acute SCI.

W. B. Edwards (✉) · K. L. Troy
Department of Kinesiology and Nutrition, University of Illinois at Chicago, 1919 W. Taylor Street, 650 AHSB, M/C 517, Chicago, IL 60621, USA
e-mail: wbedward@ucalgary.ca

T. J. Schnitzer
Department of Physical Medicine and Rehabilitation Feinberg School of Medicine, Northwestern University, Chicago, IL 60611, USA

K. L. Troy
Department of Bioengineering, University of Illinois at Chicago, Chicago, IL 60612, USA

Introduction

Bone loss is a recognized sequela of spinal cord injury (SCI). It occurs primarily at regions below the neurological lesion with little to no loss at the spine or supralesional regions [1, 2]. Mechanical unloading from the loss of motor function is an important factor in the pathogenesis of SCI related bone loss; however, metabolic, endocrine, neural, and vascular changes after SCI have also been implicated as important mediating factors [3]. Unlike primary osteoporosis, the greatest loss of bone mineral in people with SCI is observed around regions of the knee. Within the first 2 to 3 years of SCI, some 50 % of the bone mineral at the distal femur and proximal tibia is resorbed [4, 5].

In addition to complications such as heterotopic ossification [6] and kidney stone development [7], bone loss after SCI is associated with an increased rate of fragility fracture that is two times greater than the general population [8]. Consistent with the observed losses in bone mineral, fractures in individuals with SCI frequently occur around regions of the knee [9, 10]. Fractures after SCI are a source of considerable morbidity, loss of independence, and increased medical costs. Approximately 50 % of these fractures are characterized by medical complications requiring prolonged hospitalization and discharge to a second facility rather than home [11].

Bone mineral loss after SCI has been well characterized using both dual energy X-ray absorptiometry (DXA) [2, 4, 12, 13] and quantitative computed tomography (QCT) [5, 14–16]. Unfortunately, the mechanical consequence of this bone loss remains unclear. The mechanical integrity of bone will depend on parameters such as geometry, mineral distribution, material properties, and mode of loading. DXA is limited to an areal projection of integral bone mineral, and previous studies utilizing QCT to investigate SCI related bone loss have employed single-slice analyses with surrogate measures of mechanical integrity (e.g., mass-weighted moments of inertia). A better understanding of the mechanical consequence of SCI related bone loss may therefore aid in the development of preventive techniques to reduce the occurrence of fracture in this population.

The purpose of this study was to quantify changes to bone mineral, geometry, strength indices, and stiffness at the distal femur and proximal tibia in acute SCI (<1 year). To this end, a short-term prospective analysis (2.6–4.8 months depending on the subject) was performed on individuals with acute SCI using QCT analysis and patient-specific finite element (FE) modeling. We focus on acute SCI because the largest declines in bone mineral are observed during this time period [4, 5],

rendering it an important treatment window for therapeutic intervention.

Methods

Subjects

Thirteen adults with acute SCI, and medically stable in the opinion of their physiatrist, were recruited from the inpatient population at the Rehabilitation Institute of Chicago (RIC). No inclusion/exclusion criteria were based on sex, race, or ethnicity. All subjects had SCI within 4 months, were non-ambulatory, and had an American Spinal Injury Association (ASIA) impairment scale level of A, B, or C at study entry (Table 1). Pregnant females and patients with current or recent (within 12 months) use of drugs that affect bone metabolism (bisphosphonates, PTH, selective estrogen receptor modulators [SERMs]) were excluded from participation. Prior to participation, the study was approved by the necessary Institutional Review Boards and subjects provided written informed consent.

CT acquisition

Each subject received two CT scans separated by a mean of 3.5 months (range, 2.6–4.8 months), referred to hereafter as "baseline" and "follow-up" scans. All CT images were acquired on the right knee, apart from one subject with femoral fixation hardware for which images were acquired on the left knee. The CT scans were performed using a Sensation 64 Cardiac (Siemens Medical Systems, Forchheim, Germany; 120 kVp, 280 mA s, pixel resolution 0.352 mm, slice thickness 1 mm). Each scan was 30 cm in length and captured approximately 15 cm each of the distal femur and

Table 1 Subject characteristics and time post-SCI at baseline and follow-up scans

Subject	Sex	SCI level	ASIA	Age	Months post-SCI at baseline	Months post-SCI at follow-up	Months between scans
1	F	C6	B	21	1.5	4.7	3.2
2	F	C5–C6	C	64	1.0	4.9	3.9
3	M	T11	B	22	2.0	4.5	2.6
4	M	T11	B	44	2.9	6.1	3.2
5	F	T4–T5	B	21	1.4	4.4	3.0
6	M	C4	A	22	3.0	7.7	4.7
7	M	C5–C6	B	25	1.7	6.4	4.7
8	M	C4–C5	A	24	2.2	7.0	4.8
9	M	C4	B	25	1.1	3.7	2.6
10	M	C7	B	19	3.8	6.8	3.0
11	M	C5	A	27	3.1	7.7	4.7
12	F	T5	A	25	2.7	6.2	3.5
13	M	C5	B	23	1.3	4.6	3.3

proximal tibia. All CT scans included a phantom — placed on the side of, or underneath, the subjects' knee — with known calcium hydroxyapatite concentrations (QRM, Moehrendorf, Germany). The phantom served as an interscan calibration, allowing for the conversion of CT Hounsfield units to bone equivalent density ρ_{ha}.

CT image alignment and registration

The CT images were first aligned and registered using a combination of Mimics (Materialise, Leuven, Belgium) and Matlab (MathWorks, Natick, MA, USA) software. For this procedure, alignment and registration was performed separately for femora and tibiae creating two image series per scan. The native baseline images were first manually realigned along the longitudinal axis of the femur or tibia. Native follow-up images were then registered into their respective aligned baseline images using a previously reported registration procedure [17]. Analyses of three randomly rotated images from each of six different subjects suggested the registration procedure was highly accurate. For femur bones, the mean absolute error about the anterior–posterior, medial–lateral, and transverse axes were all $0.0\pm0.0°$, $0.0\pm0.0°$, and $0.0\pm0.0°$, respectively. For tibia bones, the mean absolute error about the anterior–posterior, medial–lateral, and transverse axes were $0.0\pm0.0°$, $0.0\pm0.0°$, and $0.4\pm0.5°$, respectively (note that registration errors about the transverse axes will not influence the reliability of the QCT outcome measures reported below).

QCT mineral analysis

The QCT mineral analyses were performed by a single researcher (WBE). Three regions were analyzed for each bone corresponding to 0–10 %, 10–20 %, and 20–30 % of segment length, as measured from the distal end of the femur or proximal end of the tibia (Fig. 1) [18]. These regions were chosen based on their anatomical correspondence to epiphyseal (0–10 %), metaphyseal (10–20 %), and diaphyseal (20–30 %) locations. Segment lengths were estimated from self reported stature using the proportionality constants of Drillis and Contini as cited by Winter [19]. This method of segment length estimation was chosen in place of direct stature or segment measurement due to difficulties in reliably assessing these parameters in the SCI population. What is most important with this within-subject study design is that the regions of interest correspond between respective baseline and follow-up scans.

The CT Hounsfield units were converted to bone equivalent density using a linear relationship established with the phantom. This process can result in negative bone density values for voxels comprised primarily of marrow fat [20]. Femora and tibiae were segmented from CT images using a

0.15 g/cm^3 threshold to identify the periosteal surface boundary; some manual identification was required for lower-dense bones in regions with a thin cortical shell. These regions were all located in the distal most epiphyseal region, for which, the coefficients of variance in measurement parameters were within 0.2 % at the femur and 0.6 % at the tibia (as indicated from three repeat analyses for each of six subjects from both baseline and follow-up scans, i.e., 3 analyses × 6 subjects × 2 scans=36 image series). For the epiphyseal and metaphyseal regions, we computed volumetric bone mineral density (vBMD; g/cm^3) and bone mineral content (BMC; g) for integral, cortical, and trabecular regions of bone (Fig. 1). Trabecular and cortical bone specific regions were identified using methods identical to those previously described for the proximal tibia [18]. The trabecular region was determined from a 3.5-mm, or 10-pixel, in-plane erosion of the integral bone region (i.e., all voxels contained within the periosteal surface boundary). The cortical region was determined from a Boolean subtraction of the trabecular from the integral region, followed by a thresholding of 0.35 g/cm^3 to remove any residual trabecular bone. For the diaphyseal region, only integral and cortical vBMD and BMC were computed. Here, the cortical region included all voxels within the integral region greater than 0.35 g/cm^3.

QCT geometry and strength indices

Measurements of distal femur and proximal tibia geometry and strength indices were determined using methods similar to those described for the proximal femur by Lang et al. [21]. These measures were calculated along the longitudinal axis of the bone and subsequently averaged within each region. Cross-sectional area (CSA; cm^2) was calculated as the cumulative sum of voxel area within the periosteal surface boundary. Bone volumes (BV; cm^3) of integral and cortical bone were quantified for each region and used as surrogate measures of periosteal and endosteal expansion. A compressive strength index (CSI; g^2/cm^4) was calculated as

$$CSI = iBMD^2 \cdot CSA,$$

where iBMD is the integral vBMD. Additionally, a torsional strength index (TSI; cm^3) was calculated:

$$TSI = \frac{I_x + I_y}{W} \quad
\begin{aligned}
I_x &= \frac{1}{E_c} \sum_i E_i \cdot \left(y_i - y\right)^2 \cdot dA \\
I_y &= \frac{1}{E_c} \sum_i E_i \cdot \left(x_i - x\right)^2 \cdot dA, \\
W &= 2 \cdot \sqrt{\frac{CSA}{\pi}}
\end{aligned}$$

where $(I_x + I_y)$ is the modulus weighted polar moment of inertia of the cross-section, W is the effective bone width, E_i is

Fig. 1 Frontal plane CT image slice from a representative subject illustrating integral, trabecular, and cortical regions of the distal femur and proximal tibia, which are highlighted in *yellow*. *Dotted lines* depict the partitions between epiphyseal (*Epi*), metaphyseal (*Met*) and diaphyseal (*Dia*) regions
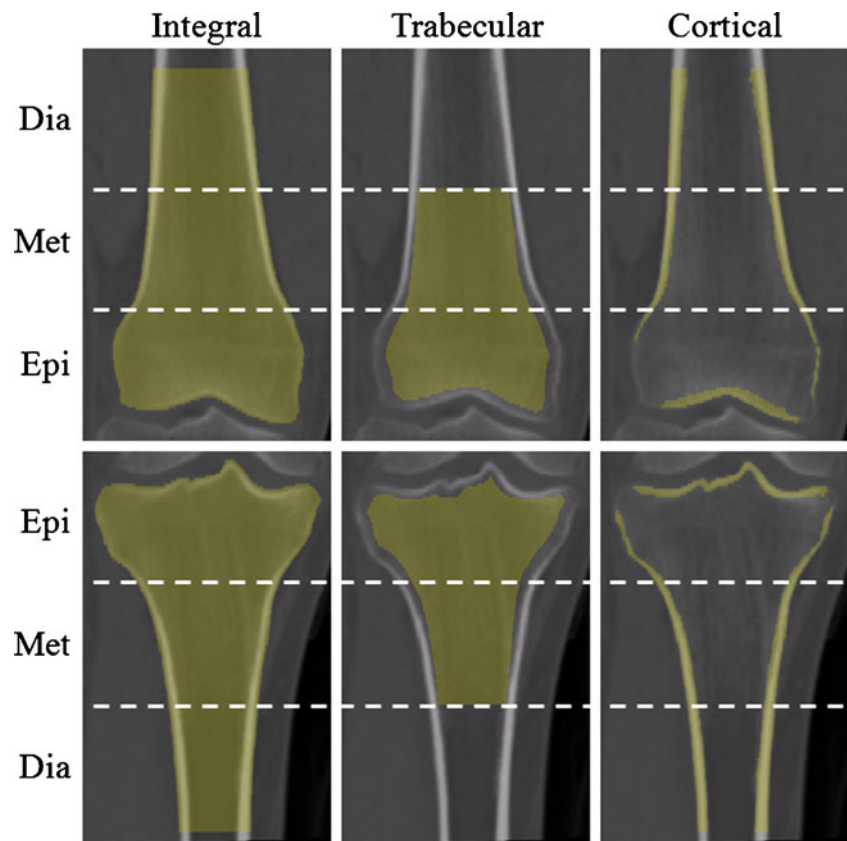
the elastic modulus for the ith voxel located at (x_i, y_i), E_c is the elastic modulus of cortical bone, and $(\overline{x}, \overline{y})$ is the modulus weighted centroid of the cross-section. Elastic moduli were determined using a density–elasticity relationship specific to proximal tibia bone [22]:

$$E_3 = 6,570\rho_{app}^{137},$$

where E_3 is expressed in MPa and ρ_{app} is the apparent density expressed in g/cm³ ($\rho_{app}=\rho_{ha}/0.626$) [23].

FE predicted stiffness

The FE method was used to calculate compressive K_c and torsional stiffness K_t for epiphyseal, metaphyseal, and diaphyseal regions of the distal femur and proximal tibia. Images were resampled to isotropic voxels with 1.5-mm edge length and segmented bones were directly converted to voxel-based FE models with linear hexahedral elements. This level of refinement was chosen following a convergence analysis examining element edge lengths ranging from 3.0 to 1.0 mm; decreasing edge length from 1.5 to 1.0 mm changed FE predicted stiffness by less than 2 %. Bone elements were assigned to one of approximately 160 linear orthotropic material properties corresponding to a bin width of 10

Hounsfield units. Elastic moduli in the axial direction E_3 was defined using the density–elasticity relationship of Rho et al. [22] (see QCT geometry and strength indices). Values of E_3 less than 0.01 MPa were assigned a new value of 0.01 MPa [24]. Anisotropy was assumed to be the same throughout with $E_1=0.574 \cdot E_3$, $E_2=0.577 \cdot E_3$, $G_{12}=0.195 \cdot E_3$, $G_{23}=0.265 \cdot E_3$, $G_{31}=0.216 \cdot E_3$, $\nu_{12}=0.427$, $\nu_{23}=0.234$, and $\nu_{31}=0.405$ [25]. Here, subscripts 1 and 2 denote the medial and anterior directions, respectively. These anisotropic definitions have illustrated excellent agreement between experimentally measured and FE predicted principal strains for a cadaveric tibia loaded in compression ($r^2=0.966$) and torsion ($r^2=0.994$) [26]. Additionally, these modeling parameters have illustrated excellent agreement between experimentally measured and FE predicted torsional stiffness ($r^2=0.949$) for 22 cadaveric proximal tibiae [18].

The FE models were subjected to either a fixed axial (compression) or torsional (internal-rotation) displacement. Surface nodes at the proximal end of femoral models and distal end of tibial models were fully constrained (Fig. 2). Displacements were applied to a reference node placed at the geometric center of, and kinematically coupled to, the distal most surface nodes of femoral models and the proximal most surface nodes of tibial models. Owing to the irregular surface at epiphyseal regions, the reference node for these models was

Fig. 2 Representative finite element (*FE*) models for epiphseal, metaphyseal, and diaphyseal regions of the distal femur (*left*) and proximal tibia (*right*). Displacement constraints are shown in *blue* and kinematic coupling constraints are shown in *yellow*
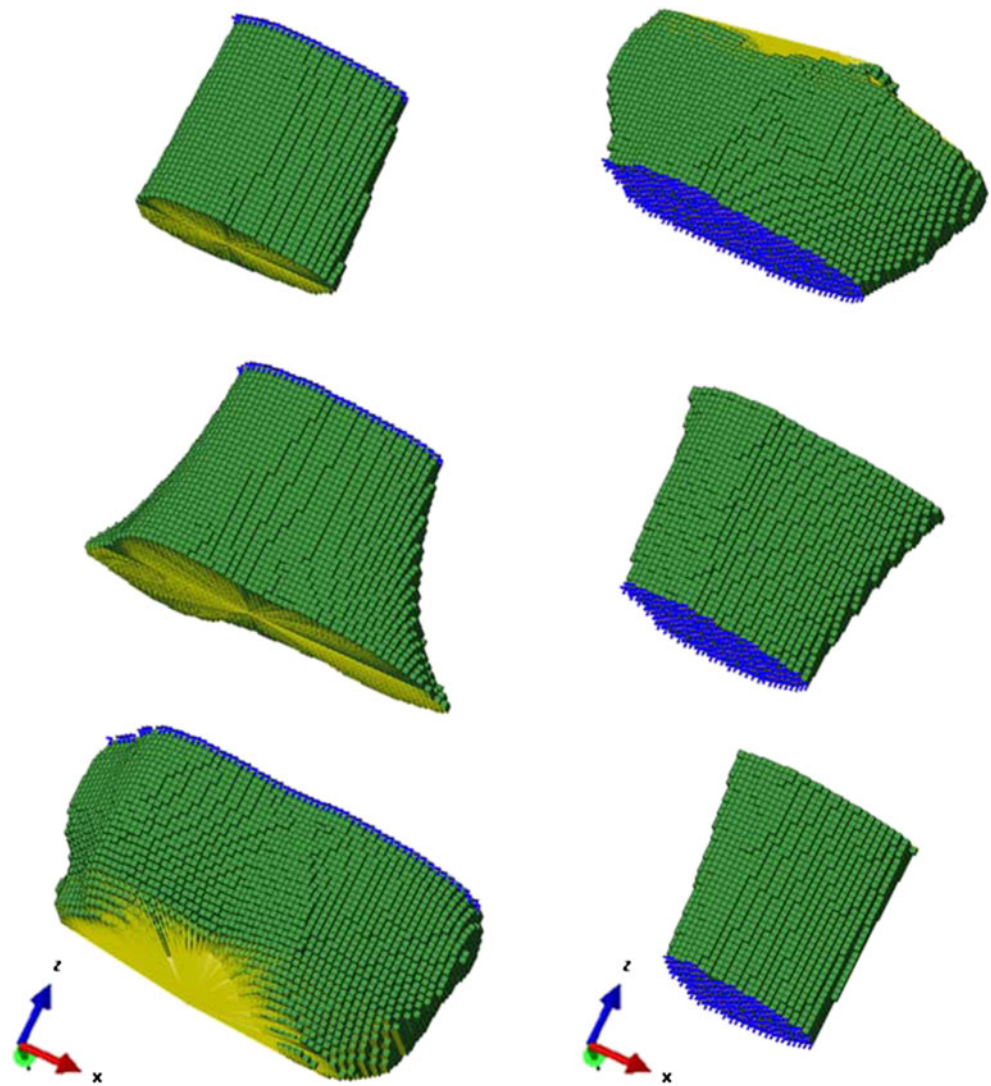
coupled to the distal most 1.5 cm of surface nodes for femoral models and the proximal most 1.5 cm of surface nodes for tibial models. All other degrees of freedom of the reference node were constrained and the reaction force, or torque, was monitored and used to calculate stiffness.

Statistical analysis

Statistical analyses were performed using SPSS software (Chicago, IL, USA). Data were examined for assumptions of normality and differences between baseline and follow-up outcome measures were examined using paired Student's *t*-tests or Wilcoxon signed-rank tests where appropriate. Due to the large number of statistical comparisons the criterion alpha level was set to 0.01. Percent changes between baseline and follow-up scans were also computed and normalized to time between baseline and follow-up scans in months.

Results

Bone mineral

During the acute period of SCI, integral bone at the distal femur illustrated mean declines ranging from 1.0 % to 3.0 % per month for integral BMC ($p \leq 0.002$) and from 0.9 % to 2.8 % per month for integral vBMD ($p \leq 0.005$), depending on the region of interest (Table 2). Trabecular BMC decreased by an average of 2.3–3.1 %/month ($p < 0.001$) and trabecular vBMD by an average of 2.0–2.7 %/month ($p < 0.001$). A 1.0–3.8 %/month mean reduction was observed for cortical BMC ($p \leq 0.004$). The mean reduction in cortical vBMD was noticeably lower (0.5–0.8 %/month), reaching significance at the epiphyseal ($p < 0.001$) and metaphyseal ($p = 0.003$) regions. A clear trend was observed in that bone mineral loss progressively decreased moving proximally away from the epiphysis (Fig. 3).

Table 2 Mean (SD) QCT measures of BMC and vBMD for integral, cortical, and trabecular components of epiphyseal (Epi), metaphyseal (Met), and diaphyseal (Dia) regions of the distal femur and proximal tibia

				Epi	Met	Dia
Distal femur	BMC (g)	Integral	Baseline	35.99 (9.69)	24.92 (6.20)	22.35 (5.82)
			Follow-up	32.37 (10.19)*	23.29 (6.08)*	21.63 (5.89)†
			Percent change/month	−3.0 (1.8)	−1.9 (1.0)	−1.0 (0.8)
		Cortical	Baseline	10.59 (3.54)	14.67 (3.67)	19.87 (5.28)
			Follow-up	8.47 (3.69)*	13.49 (3.56)*	19.21 (5.32)†
			Percent change/month	−5.8 (3.7)	−2.3 (1.4)	−1.0 (1.0)
		Trabecular	Baseline	17.64 (5.77)	7.34 (2.73)	N/A
			Follow-up	15.95 (6.09)*	6.77 (2.64)*	
			Percent change/month	−3.1 (2.1)	−2.3 (1.6)	
	vBMD (g/cm³)	Integral	Baseline	0.271 (0.032)	0.319 (0.042)	0.494 (0.058)
			Follow-up	0.244 (0.042)*	0.301 (0.044)*	0.478 (0.056)†
			Percent change/month	−2.8 (1.8)	−1.7 (1.1)	−0.9 (0.8)
		Cortical	Baseline	0.488 (0.024)	0.715 (0.041)	0.944 (0.043)
			Follow-up	0.475 (0.025)*	0.702 (0.039)†	0.926 (0.046)
			Percent change/month	−0.8 (0.4)	−0.5 (0.6)	−0.5 (0.6)
		Trabecular	Baseline	0.234 (0.035)	0.159 (0.028)	N/A
			Follow-up	0.212 (0.045)*	0.148 (0.030)*	
			Percent change/month	−2.7 (1.9)	−2.0 (1.6)	
Proximal tibia	BMC (g)	Integral	Baseline	26.72 (7.18)	23.47 (6.13)	22.40 (5.15)
			Follow-up	23.37 (7.68)*	22.37 (6.13)*	21.60 (5.04)
			Percent change/month	−3.6 (2.4)	−1.3 (1.1)	−0.4 (0.9)
		Cortical	Baseline	8.73 (2.79)	17.33 (4.04)	21.65 (5.09)
			Follow-up	7.09 (2.73)*	16.53 (4.16)†	20.84 (5.04)
			Percent change/month	−5.4 (2.9)	−1.3 (1.5)	−0.4 (1.0)
		Trabecular	Baseline	11.11 (4.02)	4.72 (2.29)	N/A
			Follow-up	9.47 (4.47)†	4.36 (2.28)†	
			Percent change/month	−4.4 (3.8)	−2.3 (1.9)	
	vBMD (g/cm³)	Integral	Baseline	0.241 (0.032)	0.393 (0.054)	0.582 (0.073)
			Follow-up	0.211 (0.046)*	0.375 (0.058)†	0.572 (0.068)
			Percent change/month	−3.4 (2.4)	−1.2 (1.3)	−0.4 (1.0)
		Cortical	Baseline	0.532 (0.024)	0.837 (0.050)	0.990 (0.046)
			Follow-up	0.521 (0.024)†	0.815 (0.058)	0.974 (0.043)
			Percent change/month	−0.6 (0.7)	−0.7 (1.2)	−0.3 (1.0)
		Trabecular	Baseline	0.174 (0.033)	0.140 (0.047)	N/A
			Follow-up	0.149 (0.049)†	0.130 (0.049)†	
			Percent change/month	−4.1 (3.8)	−2.2 (1.8)	

Statistical significance between baseline and follow-up measures are indicated by * ($p < 0.001$) and † ($p \leq 0.01$)

Integral bone at the proximal tibia illustrated mean declines ranging from 0.4 % to 3.6 % per month for integral BMC and from 0.4 % to 3.4 %/month for integral vBMD (Table 2). These changes were significant at the epiphyseal ($p < 0.001$) and metaphyseal ($p \leq 0.003$) regions. Trabecular BMC decreased by an average of 2.3–4.4 %/month ($p \leq 0.005$) and trabecular vBMD by an average of 2.2–4.7 %/month ($p \leq 0.005$). A 0.4–5.4 %/month mean reduction was observed for cortical BMC, while the mean reduction in cortical vBMD was noticeably lower (0.3–0.6 %/month). Changes in cortical BMD were significant at the epiphyseal ($p < 0.001$) and metaphyseal

($p = 0.001$) regions, while changes in cortical vBMD were only significant at the epiphyseal ($p = 0.01$) region. Similar to the femur, a clear trend was observed in that bone mineral loss progressively decreased moving distally away from the epiphysis (Fig. 3).

Geometry and strength indices

The observed declines in bone mineral at the femur were associated with a 1.8–5.4 %/month mean reduction in CSI ($p \leq 0.003$) and a 1.2–3.8 %/month mean reduction in TSI

Fig. 3 Mean relative changes/
month in QCT measures of BMC
and vBMD for integral, cortical,
and trabecular components of
epiphyseal (*Epi*), metaphyseal
(*Met*), and diaphyseal (*Dia*)
regions of the distal femur and
proximal tibia. Error bars
illustrate 1 standard deviation
(see Table 2 for significance)
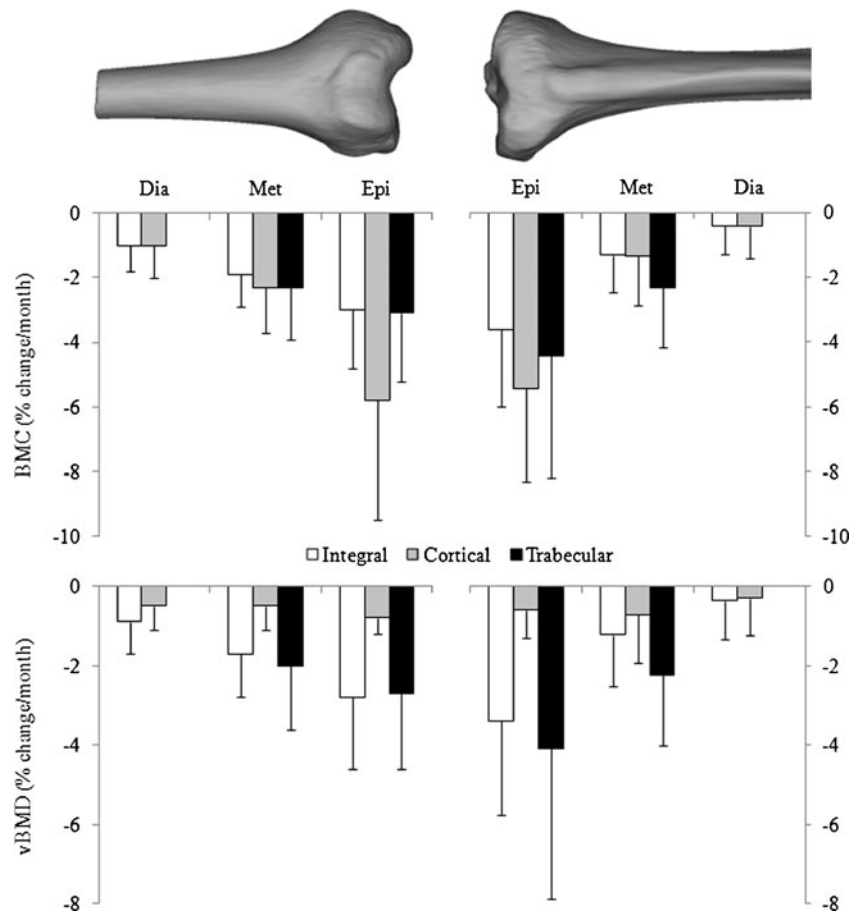
($p \leq 0.001$), depending on the region of interest (Table 3). Declines at the tibia were associated with a 0.8–6.3 %/month mean reduction in CSI and a 0.7–4.2 %/month mean reduction in TSI. These changes were significant at the epiphyseal ($p < 0.001$) and metaphyseal ($p < 0.001$) regions. Measures of CSA did not illustrate significant declines at the femur (0.1–0.3 %/month; $p \geq 0.02$) or tibia (0.1–0.3 %/month; $p \geq 0.04$). Similarly, integral BV did not illustrate significant declines at the femur (0.1–0.2 %/month; $p \geq 0.02$) or tibia (0.1–0.3 %/month; $p \geq 0.04$). On the other hand cortical BV decreased by 0.5–5.3 %/month at the femur and by 0.1–5.0 %/month at the tibia. Reductions in cortical BV were significant across all regions of the femur ($p \leq 0.003$) and the epiphyseal ($p < 0.001$) and metaphyseal ($p = 0.001$) regions of the tibia.

FE predicted stiffness

The FE predicted compressive stiffness K_c decreased by an average of 1.3–5.5 %/month ($p \leq 0.002$) across regions of the femur and by an average of 0.6–5.9 %/month ($p \leq 0.009$) across regions of the tibia (Table 3). The FE predicted torsional stiffness K_t decreased by an average of 1.3–5.0 %/month ($p < 0.001$) across regions of the femur

and by an average of 0.7–5.2 %/month ($p \leq 0.003$) across regions of the tibia.

Discussion

The mechanical consequence of bone loss associated with SCI has been difficult to interpret due to limitations in the imaging and analysis techniques previously employed. In this study, volumetric QCT analysis and patient-specific FE modeling were used to quantify changes to bone mineral, geometry, strength indices, and stiffness at the distal femur and proximal tibia over a 2.6- to 4.8-month period of acute SCI. The results illustrated a marked loss of bone mineral that was similar in magnitude at both the distal femur and proximal tibia. These losses were greatest at epiphyseal regions and were associated with large changes in measures of mechanical integrity. Reductions in QCT strength indices and FE predicted stiffness at epiphyseal regions were approximately two times greater than the observed reductions in integral vBMD.

To our knowledge, this study is the first to utilize patient-specific FE modeling to examine changes in bone stiffness following SCI. It remains unclear if these changes in stiffness are associated with similar changes in strength. Although

Table 3 Mean (SD) QCT measures of bone geometry and strength as well as FE model predicted stiffness for epiphyseal (Epi), metaphyseal (Met), and diaphyseal (Dia) regions of the distal femur and proximal tibia

			Epi	Met	Dia
Distal femur	Integral BV (cm^3)	Baseline	131.50 (24.32)	78.57 (19.17)	45.55 (11.76)
		Follow-up	130.66 (24.60)	77.78 (18.72)	45.43 (11.80)
		Percent change/month	−0.2 (0.5)	−0.3 (0.4)	−0.1 (0.2)
	Cortical BV (cm^3)	Baseline	21.44 (6.30)	20.40 (4.49)	20.96 (5.11)
		Follow-up	17.54 (7.00)*	19.09 (4.44)*	20.62 (5.10)†
		Percent change/month	−5.3 (3.7)	−1.8 (1.0)	−0.5 (0.4)
	CSA (cm^2)	Baseline	29.42 (3.68)	17.84 (3.46)	10.68 (2.08)
		Follow-up	29.23 (3.78)	17.66 (3.35)	10.35 (2.10)
		Percent change/month	−0.2 (0.5)	−0.3 (0.4)	−0.1 (0.2)
	CSI (g^2/cm^4)	Baseline	2.21 (0.70)	1.82 (0.50)	2.46 (0.67)
		Follow-up	1.82 (0.74)*	1.61 (0.49)*	2.37 (0.67)†
		Percent change/month	−5.4 (3.1)	−3.4 (1.9)	−1.8 (1.5)
	TSI (cm^3)	Baseline	4.69 (1.39)	3.43 (0.97)	2.85 (0.76)
		Follow-up	4.08 (1.41)*	3.12 (0.92)*	2.69 (0.83)†
		Percent change/month	−3.8 (2.3)	−2.5 (1.3)	−1.2 (1.0
	K_c (kN/mm)	Baseline	226.17 (49.82)	122.33 (21.91)	150.38 (22.85)
		Follow-up	183.08 (63.90)*	113.28 (20.56)*	142.90 (24.30)†
		Percent change/month	−5.5 (3.9)	−2.0 (1.6)	−1.3 (1.1)
	K_t (N m/deg)	Baseline	552.61 (162.09)	177.99 (56.81)	131.84 (42.29)
		Follow-up	458.87 (176.81)*	165.49 (52.86)*	126.03 (43.21)*
		Percent change/month	−5.0 (3.5)	−1.9 (1.7)	−1.3 (1.1)
Proximal tibia	Integral BV (cm^3)	Baseline	110.10 (20.70)	59.83 (13.84)	38.83 (8.75)
		Follow-up	109.28 (21.20)	59.52 (13.63)	38.00 (8.67)
		Percent change/month	−0.3 (0.3)	−0.1 (0.4)	−0.1 (0.4)
	Cortical BV (cm^3)	Baseline	16.30 (4.79)	20.60 (4.14)	21.86 (4.89)
		Follow-up	13.48 (4.74)*	20.11 (4.19)†	21.34 (4.82)
		Percent change/month	−5.0 (2.8)	−0.7 (0.6)	−0.1 (0.4)
	CSA (cm^2)	Baseline	25.10 (3.20)	13.44 (2.38)	8.63 (1.58)
		Follow-up	24.91 (3.36)	13.37 (2.34)	8.52 (1.53)
		Percent change/month	−0.3 (0.3)	−0.1 (0.4)	−0.1 (0.4)
	CSI (g^2/cm^4)	Baseline	1.49 (0.49)	2.10 (0.66)	2.92 (0.77)
		Follow-up	1.17 (0.53)*	1.92 (0.66)*	2.79 (072)
		Percent change/month	−6.3 (3.9)	−2.5 (2.3)	−0.8 (1.8)
	TSI (cm^3)	Baseline	2.90 (0.76)	3.28 (0.89)	2.71 (0.66)
		Follow-up	2.46 (0.80)*	3.07 (0.91)*	2.58 (0.66)
		Percent change/month	−4.2 (2.6)	−1.9 (1.8)	−0.7 (1.3)
	K_c (kN/mm)	Baseline	138.94 (35.22)	134.24 (24.61)	148.60 (23.80)
		Follow-up	110.01 (45.27)†	126.15 (26.20)†	145.00 (22.64)†
		Percent change/month	−5.9 (4.7)	−1.7 (1.8)	−0.6 (0.9)
	K_t (Nm/deg)	Baseline	313.90 (99.42)	148.67 (45.28)	99.81 (28.77)
		Follow-up	256.68 (103.17)*	140.18 (45.29)†	97.25 (28.11)†
		Percent change/month	−5.2 (3.7)	−1.6 (1.8)	−0.7 (0.9)

Statistical significance between baseline and follow-up measures are indicated by * ($p < 0.001$) and † ($p \leq 0.01$)

some studies have observed high correlations between FE predicted stiffness and fracture strength in vitro [27, 28], post-yield behavior and its contributions to strength will depend on loading mode and strain rate [29]. Further research addressing the relationship between stiffness and strength in the SCI population is therefore warranted. An interesting

finding was that similar relative reductions were observed for FE predicted stiffness and QCT strength indices (see Table 3). In fact, post-hoc correlation analyses illustrated strong relationships between these two measures. For the femur and tibia, respectively, correlations of $r=0.881$ and $r=0.945$ were observed between changes in CSI and K_c, while correlations of $r=0.884$ and $r=0.911$ were observed between changes in TSI and K_t. This finding has important implications for QCT-based studies of SCI, suggesting that surrogate measures of bone strength provide meaningful information about mechanical integrity, at least around regions of the knee.

Measures of bone loss along the periosteal surface boundary, such as integral BV and CSA, did not illustrate significant changes. On the other hand, cortical BV illustrated reductions as large as 5.3 %/month at the femur and 5.0 %/month at the tibia. These data suggest that cortical bone was lost from endosteal rather than periosteal resorption and this is consistent with previous literature suggesting that bone loss from disuse takes place through a combination of trabecular and endocortical resorption [5, 17, 21, 30, 31]. A clear trend was observed in that bone mineral loss progressively decreased moving from the epiphyses towards the diaphyses. This phenomenon is the probable explanation for the fact that fractures in this population dominate in the more distal regions of the femur and proximal regions of the tibia as opposed to the shafts [10, 32]. The reason that bone loss after SCI is regionally specific is unclear, but it has been hypothesized that the increased surface/volume ratio towards the ends of long bones allows for greater osteoclastic resorption [16, 31]. Additionally, recent work utilizing a Botox-induced disuse murine model suggests there may be different osteoclastogenic events mediating bone loss at the ends and shafts of long bones [33]. Specifically, this model indicates an initial resorption response within the proximal tibia caused by basal osteoclast activity, with a secondary wave of bone resorption in the diaphysis driven by osteoclastogenisis within the marrow space.

We have recently described bone mineral loss at the proximal femur in acute SCI [17]. During the same period, individuals from the present study lost proximal femur integral, trabecular, and cortical BMC at rates of 2.7–3.3 %/month, 3.1–4.7 %/month, and 3.9–4.0 %/month, respectively. Proximal femur integral, trabecular, and cortical vBMD were lost at rates of 2.5–3.1 %/month, 2.8–4.4 %/month, and 0.8–1.0 %/month, respectively. These relative rates of reduction in bone mineral are similar in magnitude to the reductions observed at epiphyseal regions of the distal femur and proximal tibia. The literature suggests the establishment of a new bone-metabolic steady-state in chronic SCI approximately 25 % and 50 % less than normal at the hip and knee, respectively [1, 4, 12]. Therefore, it is likely that bone steady-state after SCI is established at the hip first, as opposed to the knee, or that a discrepancy in the relative rates

of bone mineral decline ensues sometime after the window of acute SCI examined herein. A better understanding of the mechanism(s) behind these potential site-specific differences in bone loss patterns may help to identify novel therapies for attenuating or reversing bone loss after SCI.

This study is limited by the error inherent to QCT analysis, much of which is related to partial volume effects caused by the limited resolution of the clinical CT scan relative to the thin cortical shell [34] — especially in the epiphyseal region. Partial volume effects in the vicinity of a thin cortical shell could manifest as lower dense bone that would mistakenly be considered residual trabecular bone in the cortical region analysis. This limitation of the analysis procedure is readily observed in Fig. 1, but it is important to note that both baseline and follow-up images would be subject to this error in the same manner. The FE modeling parameters used in this study have been previously validated for proximal tibia cadaveric bones loaded in torsion [18]. However, these modeling parameters have not been validated for proximal tibia bones loaded in axial compression, or under any mode of loading for the distal femur. Particular attention should therefore be placed on the observed relative changes in stiffness between baseline and follow-up scans rather than absolute values.

The inclusion of individuals during the first few months of SCI is a strength of the study, however, some difficulty was met obtaining follow-up CT scans at a consistent length of time after baseline. Much of the between-subject variation in time between baseline and follow-up scans was unavoidable because many subjects were outpatients scattered throughout the Midwest at the time of follow-up and arrangements were made to obtain scans during return visits with RIC physiatrists nearest 12 weeks after study entry. To control for this variation, relative changes in outcome measures were normalized to months between baseline and follow-up scans. Our sample population was skewed towards young males, which limits the generalizability of our findings to females or older adults with acute SCI. On the other hand, our sample population was quite characteristic of the large majority of individuals with SCI; over 80 % are male and some 50–70 % of new cases occur in persons aged 15–35 years [35].

The findings from this study have important clinical implications for the treatment of SCI related bone loss. During the acute period of SCI, we observed a marked loss of bone mineral due to a combination of trabecular and endocortical resorption. Therefore, it is important that therapeutic interventions are implemented soon after injury and that both trabecular and cortical bone mineral preservation is targeted. Reductions in bone mineral were most pronounced at epiphyseal regions of the knee, reaching magnitudes as high as 4.7 %/month and 5.4 %/month for trabecular and cortical bone mineral, respectively. Thus, mechanical loading interventions aimed at preventing bone loss after SCI should target the epiphyseal regions of the distal femur and proximal

tibia when possible. Finally, changes in mechanical integrity, as evidenced by QCT strength indices and FE predicted stiffness, were as much as 2-fold greater than changes in integral BMD. It is important that therapists and clinicians utilizing densitometric measures to monitor bone health in people with SCI are aware of this potential discrepancy.

In summary, individuals with acute SCI experienced a rapid and substantial loss of bone mineral at the distal femur and proximal tibia through a combination of trabecular and endocortical resorption. The observed reductions in bone mineral were largest at epiphyseal regions and progressively decreased moving towards diaphyseal regions. This specific pattern of bone loss had large mechanical consequences that may, at least in part, help explain the large prevalence and distribution of fragility fracture after SCI. Studies examining the efficacy of targeted therapeutic interventions to reverse or halt SCI related bone loss are thus warranted.

References

1. Dauty M, Perrouin Verbe B, Maugars Y, Dubois C, Mathe JF (2000) Supralesional and sublesional bone mineral density in spinal cord-injured patients. Bone 27:305–309
2. Zehnder Y, Luthi M, Michel D, Knecht H, Perrelet R, Neto I, Kraenzlin M, Zach G, Lippuner K (2004) Long-term changes in bone metabolism, bone mineral density, quantitative ultrasound parameters, and fracture incidence after spinal cord injury: a cross-sectional observational study in 100 paraplegic men. Osteoporos Int 15:180–189. doi:10.1007/s00198-003-1529-6
3. Jiang SD, Dai LY, Jiang LS (2006) Osteoporosis after spinal cord injury. Osteoporos Int 17:180–192. doi:10.1007/s00198-005-2028-8
4. Biering-Sorensen F, Bohr HH, Schaadt OP (1990) Longitudinal study of bone mineral content in the lumbar spine, the forearm and the lower extremities after spinal cord injury. Eur J Clin Invest 20:330–335
5. Eser P, Frotzler A, Zehnder Y, Wick L, Knecht H, Denoth J, Schiessl H (2004) Relationship between the duration of paralysis and bone structure: a pQCT study of spinal cord injured individuals. Bone 34:869–880. doi:10.1016/j.bone.2004.01.001
6. Bravo-Payno P, Esclarin A, Arzoz T, Arroyo O, Labarta C (1992) Incidence and risk factors in the appearance of heterotopic ossification in spinal cord injury. Paraplegia 30:740–745. doi:10.1038/sc.1992.142
7. Chen Y, DeVivo MJ, Roseman JM (2000) Current trend and risk factors for kidney stones in persons with spinal cord injury: a longitudinal study. Spinal Cord 38:346–353
8. Vestergaard P, Krogh K, Rejnmark L, Mosekilde L (1998) Fracture rates and risk factors for fractures in patients with spinal cord injury. Spinal Cord 36:790–796
9. Garland DE, Adkins RH (2001) Bone loss at the knee in spinal cord injury. Top Spinal Cord Inj Rehabil 6:37–46
10. Rogers T, Shokes LK, Woodworth PH (2005) Pathologic extremity fracture care in spinal cord injury. Top Spinal Cord Inj Rehabil 11:70–78
11. Morse LR, Battaglino RA, Stolzmann KL, Hallett LD, Waddimba A, Gagnon D, Lazzari AA, Garshick E (2009) Osteoporotic fractures and hospitalization risk in chronic spinal cord injury. Osteoporos Int 20:385–392. doi:10.1007/s00198-008-0671-6
12. Biering-Sorensen F, Bohr HH, Schaadt OP (1988) Bone mineral content of the lumbar spine and lower extremities years after spinal cord lesion. Paraplegia 26:293–301
13. Garland DE, Stewart CA, Adkins RH, Hu SS, Rosen C, Liotta FJ, Weinstein DA (1992) Osteoporosis after spinal cord injury. J Orthop Res 10:371–378. doi:10.1002/jor.1100100309
14. Dudley-Javoroski S, Shields RK (2010) Longitudinal changes in femur bone mineral density after spinal cord injury: effects of slice placement and peel method. Osteoporos Int 21:985–995. doi:10.1007/s00198-009-1044-5
15. Frotzler A, Berger M, Knecht H, Eser P (2008) Bone steady-state is established at reduced bone strength after spinal cord injury: a longitudinal study using peripheral quantitative computed tomography (pQCT). Bone 43:549–555. doi:10.1016/j.bone.2008.05.006
16. Rittweger J, Goosey-Tolfrey VL, Cointry G, Ferretti JL (2010) Structural analysis of the human tibia in men with spinal cord injury by tomographic (pQCT) serial scans. Bone 47:511–518. doi:10.1016/j.bone.2010.05.025
17. Edwards WB, Schnitzer TJ, Troy KL (2013) Bone mineral loss at the proximal femur in acute spinal cord injury. Osteoporos Int. doi:10.1007/s00198-013-2323-8
18. Edwards WB, Schnitzer TJ, Troy KL (2013) Torsional stiffness and strength of the proximal tibia are better predicted by finite element models than DXA or QCT. J Biomech. doi:10.1016/j.jbiomech.2013.04.016
19. Winter DA (1990) Biomechanics and motor control of human movement. John Wiley & Sons, New York
20. Marshall LM, Lang TF, Lambert LC, Zmuda JM, Ensrud KE, Orwoll ES, Osteoporotic Fractures in Men (MrOS) Research Group (2006) Dimensions and volumetric BMD of the proximal femur and their relation to age among older U.S. men. J Bone Miner Res 21:1197–1206. doi:10.1359/jbmr.060506
21. Lang T, LeBlanc A, Evans H, Lu Y, Genant H, Yu A (2004) Cortical and trabecular bone mineral loss from the spine and hip in long-duration spaceflight. J Bone Miner Res 19:1006–1012. doi:10.1359/JBMR.040307
22. Rho JY, Hobatho MC, Ashman RB (1995) Relations of mechanical properties to density and CT numbers in human bone. Med Eng Phys 17:347–355
23. Dalstra M, Huiskes R, Odgaard A, van Erning L (1993) Mechanical and textural properties of pelvic trabecular bone. J Biomech 26:523–535
24. Keyak JH, Rossi SA, Jones KA, Les CM, Skinner HB (2001) Prediction of fracture location in the proximal femur using finite element models. Med Eng Phys 23:657–664
25. Rho JY (1996) An ultrasonic method for measuring the elastic properties of human tibial cortical and cancellous bone. Ultrasonics 34:777–783
26. Gray HA, Taddei F, Zavatsky AB, Cristofolini L, Gill HS (2008) Experimental validation of a finite element model of a human cadaveric tibia. J Biomech Eng 130:031016. doi:10.1115/1.2913335
27. Cody DD, Gross GJ, Hou FJ, Spencer HJ, Goldstein SA, Fyhrie DP (1999) Femoral strength is better predicted by finite element models than QCT and DXA. J Biomech 32:1013–1020
28. Crawford RP, Cann CE, Keaveny TM (2003) Finite element models predict in vitro vertebral body compressive strength better than quantitative computed tomography. Bone 33:744–750

29. Hansen U, Zioupos P, Simpson R, Currey JD, Hynd D (2008) The effect of strain rate on the mechanical properties of human cortical bone. J Biomech Eng 130:011011. doi:10.1115/1.2838032

30. Ito M, Matsumoto T, Enomoto H, Tsurusaki K, Hayashi K (1999) Effect of nonweight bearing on tibial bone density measured by QCT in patients with hip surgery. J Bone Miner Metab 17:45–50

31. Rittweger J, Simunic B, Bilancio G, De Santo NG, Cirillo M, Biolo G, Pisot R, Eiken O, Mekjavic IB, Narici M (2009) Bone loss in the lower leg during 35 days of bed rest is predominantly from the cortical compartment. Bone 44:612–618. doi:10.1016/j.bone.2009.01.001

32. Eser P, Frotzler A, Zehnder Y, Denoth J (2005) Fracture threshold in the femur and tibia of people with spinal cord injury as determined by peripheral quantitative computed tomography. Arch Phys Med Rehabil 86:498–504. doi:10.1016/j.apmr.2004.09.006

33. Ausk BJ, Gross TS (2012) Metaphyseal and diaphyseal bone loss following transient muscle paralysis are distinct osteoclastogenic events. Proceedings of the American Society of Biomechanics 36th Annual Meeting; 2012 Aug 15–18, Gainesville, FL. http://www.asbweb.org/conferences/2012/abstracts/200.pdf

34. Prevrhal S, Engelke K, Kalender WA (1999) Accuracy limits for the determination of cortical width and density: the influence of object size and CT imaging parameters. Phys Med Biol 44:751–764

35. Centers for Disease Control and Prevention (2010) Spinal cord injury (SCI): fact sheet. http://www.cdc.gov/traumaticbraininjury/scifacts.html. Accessed 6 September 2012